Article

Solid-State NMR Spectroscopy Applied to a Chimeric Potassium Channel in Lipid Bilayers

Robert Schneider, Christian Ader, Adam Lange, Karin Giller, Sönke Hornig, Olaf Pongs, Stefan Becker, and Marc Baldus

J. Am. Chem. Soc., **2008**, 130 (23), 7427-7435 • DOI: 10.1021/ja800190c • Publication Date (Web): 14 May 2008

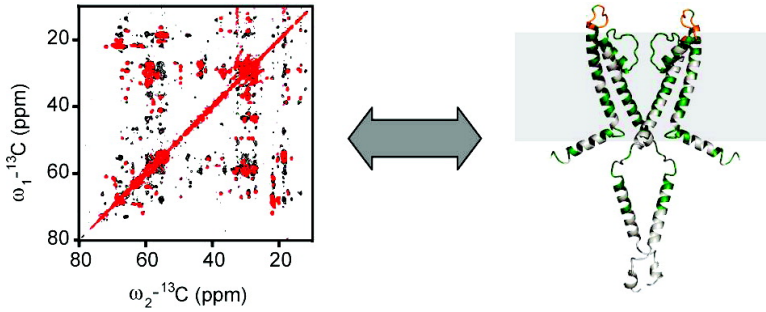

More About This Article

Additional resources and features associated with this article are available within the HTML version:

- Supporting Information
- Links to the 1 articles that cite this article, as of the time of this article download
- Access to high resolution figures
- Links to articles and content related to this article
- Copyright permission to reproduce figures and/or text from this article

View the Full Text HTML

J|A|C|S
ARTICLES

Published on Web 05/14/2008

Solid-State NMR Spectroscopy Applied to a Chimeric Potassium Channel in Lipid Bilayers†

Robert Schneider,‡ Christian Ader,‡ Adam Lange,‡,§ Karin Giller,‡ Sönke Hornig,|| Olaf Pongs,|| Stefan Becker,‡ and Marc Baldus*,‡

Department of NMR-based Structural Biology, Max Planck Institute for Biophysical Chemistry, Am Fassberg 11, 37077 Göttingen, and Institut für Neurale Signalverarbeitung, Zentrum für Molekulare Neurobiologie, Universität Hamburg, Falkenried 94, 20251 Hamburg, Germany

Received January 9, 2008; E-mail: maba@mpibpc.mpg.de

Abstract: We show that solid-state NMR can be used to investigate the structure and dynamics of a chimeric potassium channel, KcsA-Kv1.3, in lipid bilayers. Sequential resonance assignments were obtained using a combination of $^{15}N-^{13}C$ and $^{13}C-^{13}C$ correlation experiments conducted on fully labeled and reverse-labeled as well as C-terminally truncated samples. Comparison of our results with those from X-ray crystallography and solution-state NMR in micelles on the closely related KcsA K^+ channel provides insight into the mechanism of ion channel selectivity and underlines the important role of the lipid environment for membrane protein structure and function.

Introduction

Studying membrane protein structure and dynamics is intimately linked to the understanding of principal biological processes such as protein synthesis, transport, and signal transduction. X-ray crystallography has made significant progress in determining membrane protein structures[1,2] and provided unprecedented insight into biological processes such as ion selectivity and conduction or protein secretion.[3,4] On the other hand, physical interactions between membrane proteins and lipids can be essential to a large variety of cellular processes,[5–7] and protein functionality is often strongly linked to the surrounding bilayer environment.[2,6,8] Such interactions may extend beyond specific binding events of individual lipid molecules seen in X-ray structures,[9] and relating crystal structures to protein function in membranes can be compromised by molecular packing effects in crystals.[10,11]

Alternatively, nuclear magnetic resonance (NMR) represents a spectroscopic technique to study molecular structure in a noncrystalline environment and has been applied to study structural aspects of membrane and membrane−protein systems for a long time (see, e.g., refs 12–15). When detergents are employed to mimic the membrane environment, solution-state NMR methods are used to determine 3D protein structures, in particular of those involving β-barrel proteins (see, e.g., refs 16 and 17). In several cases, NMR data obtained under such conditions have been related to functional aspects of membrane-embedded proteins (for a recent review, see, e.g., ref 18). However, the choice of the micelle environment has been shown to impact protein stability, and different micellar preparations can lead to variations in NMR signal patterns.[18,19] Alternatively, solid-state NMR (ssNMR) allows for the study of molecular structures in lipid bilayers where protein structure and functionality are often most easily maintained. Macroscopically aligned samples have been used to determine entire 3D structures[13] or complement micelle-based solution-state NMR data.[19] In parallel, ssNMR has been combined with magic-angle

† Presented in part at the 5th Alpine Conference on Solid-State NMR, Sept 9−13, 2007, Chamonix, France.

‡ Max Planck Institute for Biophysical Chemistry.

§ Current address: Laboratory of Physical Chemistry, ETH Zürich, Wolfgang-Pauli-Str. 10, 8093 Zürich, Switzerland.

|| Universität Hamburg.

(1) White, S. H. *Protein Sci.* **2004**, *13*, 1948–1949.
(2) Bowie, J. U. *Nature* **2005**, *438*, 581–589.
(3) MacKinnon, R. *Angew. Chem., Int. Ed.* **2004**, *43*, 4265–4277.
(4) Papanikou, E.; Karamanou, S.; Economou, A. *Nat. Rev. Microbiol.* **2007**, *5*, 839–851.
(5) Lee, A. G. *Biochim. Biophys. Acta (BBA)−Biomembranes* **2004**, *1666*, 62–87.
(6) Matthews, E. E.; Zoonens, M.; Engelman, D. M. *Cell* **2006**, *127*, 447–450.
(7) Killian, J. A.; Nyholm, T. K. M. *Curr. Opin. Struct. Biol.* **2006**, *16*, 473–479.
(8) Klare, J. P.; Bordignon, E.; Doebber, M.; Fitter, J.; Kriegsmann, J.; Chizhov, I.; Steinhoff, H. J.; Engelhard, M. *J. Mol. Biol.* **2006**, *356*, 1207–1221.
(9) Palsdottir, H.; Hunte, C. *Biochim. Biophys. Acta (BBA)−Biomembranes* **2004**, *1666*, 2–18.
(10) Moukhametzianov, R.; Klare, J. P.; Efremov, R.; Baeken, C.; Gäppner, A.; Labahn, J.; Engelhard, M.; Büldt, G.; Gordeliy, V. I. *Nature* **2006**, *440*, 115–119.
(11) Schertler, G. F. X. *Curr. Opin. Struct. Biol.* **2005**, *15*, 408–415.
(12) Harbison, G. S.; Smith, S. O.; Pardoen, J. A.; Courtin, J. M. L.; Lugtenburg, J.; Herzfeld, J.; Mathies, R. A.; Griffin, R. G. *Biochemistry* **1985**, *24*, 6955–6962.
(13) Cross, T. A.; Opella, S. J. *Curr. Opin. Struct. Biol.* **1994**, *4*, 574–581.
(14) Smith, S. O.; Aschheim, K.; Groesbeek, M. *Q. Rev. Biophys.* **1996**, *29*, 395–449.
(15) MacKenzie, K. R.; Prestegard, J. H.; Engelman, D. M. *Science* **1997**, *276*, 131–133.
(16) Tamm, L. K.; Liang, B. *Prog. Nucl. Magn. Reson. Spectrosc.* **2006**, *48*, 201–210.
(17) Sanders, C. R.; Hoffmann, A. K.; Grayn, D. N.; Keyes, M. H.; Ellis, C. D. *ChemBioChem* **2004**, *5*, 423–426.
(18) Poget, S. F.; Girvin, M. E. *Biochim. Biophys. Acta (BBA)−Biomembranes* **2007**, *1768*, 3098–3106.
(19) Franzin, C. M.; Gong, X.-M.; Thai, K.; Yu, J.; Marassi, F. M. *Methods* **2007**, *41*, 398–408.

spinning (MAS[20]) to study ligand binding,[21–24] and 3D structures of membrane-associated polypeptides have been studied (see, e.g., refs 25 and 26). While significant progress has been obtained in the spectral assignment of globular proteins,[27–32] sequential resonance assignments or structural studies of larger, membrane-embedded proteins by solid-state NMR have been scarce.[33,34]In addition to limitations in the signal-to-noise ratio, such studies are complicated by the length of the amino acid sequence, the high repetitiveness of hydrophobic residues, and the limited spectral resolution arising from the dominant influence of a single type of regular secondary structure. In principle, spectral crowding can be reduced by multidimensional correlation spectroscopy[35] and advanced labeling approaches.[34,36–38] In addition, we have shown that reverse ^{13}C and ^{15}N labeling[39,40] and the application of ssNMR spectroscopic methods that separate signals stemming from mobile and static protein regions can be used to simplify the structural analysis of membrane-associated proteins.[41,42]

While these studies involved α-helical proteins that contain larger, flexible domains outside the membrane, we here investigate the utility of MAS-based ssNMR methods to study the potassium ion channel KcsA-Kv1.3, a tetramer encompassing 4×160 residues in a membrane environment. Compared to the KcsA channel first identified in the Gram-positive bacterium *Streptomyces lividans*,[43] KcsA-Kv1.3 differs by 11 amino acids, predominantly found in the pore region of the channel, which make it a high-affinity receptor for scorpion toxins, similar to the human Kv1.3 channel.[44,45] For the closely related KcsA K^+ channel, X-ray structures exist for the transmembrane and extracellular regions.[46] Structural information on the cytoplasmic domains was obtained by combining X-ray results with EPR data on spin-labeled variants of the full-length KcsA channel,[47] speaking against the existence of large protein segments that exhibit fast molecular motion. For KcsA-Kv1.3, we have previously studied the binding of kaliotoxin (KTX) in lipid bilayers and reported resonance assignments for 19 residues in the turret and selectivity filter regions of the channel.[24,48] In the following, we investigate whether dipolar-based two- and three-dimensional ssNMR correlation experiments conducted on reverse labeled and C-terminally truncated channel versions can be used to study this 4×160 residue protein in lipid bilayers. We report resonance assignments at pH 7.5, study structural and dynamical aspects in lipid bilayers, and compare our results to those obtained on KcsA crystals and in NMR studies of KcsA constructs in micelles.[49,50] These results underline the potential of ssNMR to study larger, membrane-embedded proteins in a functional bilayer environment and reveal structural differences of a protein studied in a crystal lattice, in detergent micelles, and in the lipid bilayer.

Materials and Methods

Expression and Purification of ^{13}C,^{15}N-Labeled KcsA-Kv1.3 Constructs. Experiments were carried out using ^{13}C,^{15}N uniformly labeled (in the following [U]KcsA-Kv1.3) and reverse-labeled (containing leucine, valine, tryptophan, and tyrosine in natural abundance, [R]KcsA-Kv1.3) versions of the full-length channel. In addition, a sample truncated after residue 125 by chymotrypsin digestion was used to assist in identification of C-terminal residues (denoted by [T]KcsA-Kv1.3). Isotope labeling and reconstitution in lipid bilayers were done as described previously.[24] Briefly, channel protein was solubilized using *n*-decyl β-D-maltopyranoside (DM) (Calbiochem) as the detergent, purified on Ni^{2+}−nitrilotriacetic acid agarose, and eluted with 100 mM sodium phosphate, pH 7.8, containing 150 mM KCl, 400 mM imidazole, and 4 mM DM. This buffer was then exchanged on a desalting column (HiPrep 26/10, Amersham) against 50 mM sodium phosphate, pH 7.4, 50 mM NaCl, and 4 mM DM. Reconstitution in liposomes was performed by adding soybean asolectin (Fluka) resuspended in the same buffer at a 100/1 asolectin/KcsA-Kv1.3 molar ratio. Proteoliposomes were harvested by centrifugation at 45 000 rpm (Ti50).

(20) Andrew, E. R.; Bradbury, A.; Eades, R. G. *Nature* **1958**, *182*, 1659.
(21) Creemers, A. F. L.; Kiihne, S.; Bovee-Geurts, P. H. M.; DeGrip, W. J.; Lugtenburg, J.; de Groot, H. J. M. *Proc. Natl. Acad. Sci. U.S.A.* **2002**, *99*, 9101–9106.
(22) Luca, S.; White, J. F.; Sohal, A. K.; Filippov, D. V.; van Boom, J. H.; Grisshammer, R.; Baldus, M. *Proc. Natl. Acad. Sci. U.S.A.* **2003**, *100*, 10706–10711.
(23) Krabben, L.; van Rossum, B.-J.; Castellani, F.; Bocharov, E.; Schulga, A. A.; Arseniev, A. S.; Weise, C.; Hucho, F.; Oschkinat, H. *FEBS Lett.* **2004**, *564*, 319–324.
(24) Lange, A.; Giller, K.; Hornig, S.; Martin-Eauclaire, M.-F.; Pongs, O.; Becker, S.; Baldus, M. *Nature* **2006**, *440*, 959–962.
(25) Andronesi, O. C.; Pfeifer, J. R.; Al-Momani, L.; Özdirekcan, S.; Rijkers, D. T. S.; Angerstein, B.; Luca, S.; Koert, U.; Killian, J. A.; Baldus, M. *J. Biomol. NMR* **2004**, *30*, 253–265.
(26) Todokoro, Y.; Yumen, I.; Fukushima, K.; Kang, S.-W.; Park, J.-S.; Kohno, T.; Wakamatsu, K.; Akutsu, H.; Fujiwara, T. *Biophys. J.* **2006**, *91*, 1368–1379.
(27) Straus, S. K.; Bremi, T.; Ernst, R. R. *J. Biomol. NMR* **1998**, *12*, 39–50.
(28) Pauli, J.; Baldus, M.; van Rossum, B.; de Groot, H.; Oschkinat, H. *ChemBioChem* **2001**, *2*, 272–281.
(29) Detken, A.; Hardy, E. H.; Ernst, M.; Kainosho, M.; Kawakami, T.; Aimoto, S.; Meier, B. H. *J. Biomol. NMR* **2001**, *20*, 203–221.
(30) Böckmann, A.; Lange, A.; Galinier, A.; Luca, S.; Giraud, N.; Heise, H.; Juy, M.; Montserret, R.; Penin, F.; Baldus, M. *J. Biomol. NMR* **2003**, *27*, 323–339.
(31) Igumenova, T. I.; Wand, A. J.; McDermott, A. E. *J. Am. Chem. Soc.* **2004**, *126*, 5323–5331.
(32) Seidel, K.; Etzkorn, M.; Heise, H.; Becker, S.; Baldus, M. *ChemBioChem* **2005**, *6*, 1638–1647.
(33) Egorova-Zachernyuk, T. A.; Hollander, J.; Fraser, N.; Gast, P.; Hoff, A. J.; Cogdell, R.; de Groot, H. J. M.; Baldus, M. *J. Biomol. NMR* **2001**, *19*, 243–253.
(34) van Gammeren, A. J.; Hulsbergen, F. B.; Hollander, J. G.; de Groot, H. J. M. *J. Biomol. NMR* **2004**, *30*, 267–274.
(35) Ernst, R. R.; Bodenhausen, G.; Wokaun, A. *Principles of Nuclear Magnetic Resonance in One and Two Dimensions*; Clarendon Press: Oxford, U.K., 1987.
(36) Castellani, F.; van Rossum, B.; Diehl, A.; Schubert, M.; Rehbein, K.; Oschkinat, H. *Nature* **2002**, *420*, 98–102.
(37) Kainosho, M.; Torizawa, T.; Iwashita, Y.; Terauchi, T.; Mei Ono, A.; Güntert, P. *Nature* **2006**, *440*, 52–57.
(38) Hiller, M.; Krabben, L.; Vinothkumar, K. R.; Castellani, F.; van Rossum, B. J.; Kuhlbrandt, W.; Oschkinat, H. *ChemBioChem* **2005**, *6*, 1679–1684.
(39) Vuister, G. W.; Kim, S. J.; Wu, C.; Bax, A. *J. Am. Chem. Soc.* **1994**, *116*, 9206–9210.
(40) Heise, H.; Hoyer, W.; Becker, S.; Andronesi, O. C.; Riedel, D.; Baldus, M. *Proc. Natl. Acad. Sci. U.S.A.* **2005**, *102*, 15871–15876.
(41) Andronesi, O. C.; Becker, S.; Seidel, K.; Heise, H.; Young, H. S.; Baldus, M. *J. Am. Chem. Soc.* **2005**, *127*, 12965–12974.
(42) Etzkorn, M.; Martell, S.; Andronesi, Ovidiu C.; Seidel, K.; Engelhard, M.; Baldus, M. *Angew. Chem., Int. Ed.* **2007**, *46*, 459–462.
(43) Schrempf, H.; Schmidt, O.; Kummerlen, R.; Hinnah, S.; Muller, D.; Betzler, M.; Steinkamp, T.; Wagner, R. *EMBO J.* **1995**, *14*, 5170–5178.
(44) Legros, C.; Pollmann, V.; Knaus, H. G.; Farrell, A. M.; Darbon, H.; Bougis, P. E.; Martin-Eauclaire, M. F.; Pongs, O. *J. Biol. Chem.* **2000**, *275*, 16918–16924.
(45) Legros, C.; Schulze, C.; Garcia, M. L.; Bougis, P. E.; Martin-Eauclaire, M. F.; Pongs, O. *Biochemistry* **2002**, *41*, 15369–15375.
(46) Zhou, Y. F.; Morais-Cabral, J. H.; Kaufman, A.; MacKinnon, R. *Nature* **2001**, *414*, 43–48.
(47) Cortes, D. M.; Cuello, L. G.; Perozo, E. *J. Gen. Physiol.* **2001**, *117*, 165–180.
(48) Lange, A.; Giller, K.; Pongs, O.; Becker, S.; Baldus, M. *J. Recept. Signal Transduction Res.* **2006**, *26*, 379–393.
(49) Chill, J. H.; Louis, J. M.; Miller, C.; Bax, A. *Protein Sci.* **2006**, *15*, 684–698.
(50) Baker, K. A.; Tzitzilonis, C.; Kwiatkowski, W.; Choe, S.; Riek, R. *Nat. Struct. Mol. Biol.* **2007**, *14*, 1089–1095.

Samples were packed in standard 4 mm MAS rotors using protein quantities of 10−20 mg.

Solid-State NMR Experiments and Analysis. All NMR experiments were conducted using 4 mm triple-resonance ^{1}H, ^{13}C, and ^{15}N probeheads at static magnetic fields of 14.1 and 18.8 T corresponding to 600 and 800 MHz proton resonance frequencies (Bruker Biospin, Karlsruhe, Germany). Previous experiments have shown that ^{1}H evolution and detection periods provide limited resolution, even if homonuclear proton−proton decoupling sequences are applied.[48] Hence, $^{13}C-^{13}C$ and $^{15}N-^{13}C$ two- and three-dimensional correlation experiments (see, e.g., ref 51 for further details) were performed on reverse-labeled and fully labeled samples at varying temperatures, corresponding to the liquid crystalline (sample temperature 2−12 °C) and gel phase (−5 to −20 °C) states of the lipid bilayer. $^{13}C-^{13}C$ mixing was accomplished by proton-driven spin diffusion under weak coupling conditions (PDSD-WC) at MAS speeds close to the rotational resonance condition for Cα and C′ resonances.[52] $^{15}N-^{13}C$ transfers typically involved SPECIFIC-CP[53,54] transfer units of 1.5−4.5 ms, followed by homonuclear $^{13}C-^{13}C$ DARR[55] mixing of up to 25 ms. CHHC experiments[56] were recorded with 250 and 500 μs longitudinal proton−proton mixing times. Short CPs before and after $^{1}H-^{1}H$ mixing were set to 80 μs. 2D spectra were typically recorded using 1280−1536 acquisition data points in the direct dimension and 384, 45, or 170 acquisition data points in the indirect dimension for $^{13}C-^{13}C$, $^{15}N-^{13}C$, or CHHC spectra, respectively, and processed using 1024 × 1024 data points. Three-dimensional NCOCA data were recorded with 3 ms evolution times in indirect ^{15}N and ^{13}C dimensions, using 21, 19, and 1024 acquisition data points in F1, F2, and F3 dimensions, respectively, and processed using 512 × 256 × 1024 data points. Spectra were processed in XWinNMR or Topspin (Bruker Biospin) and analyzed with Sparky (T. D. Goddard and D. G. Kneller, SPARKY 3, University of California, San Francisco).

Generation of the KcsA-Kv1.3 Structural Model. A structural model for the chimeric channel was generated using the KcsA-Kv1.3 protein sequence, the crystal structure of residues 22−124 of KcsA[46] (PDB ID 1K4C), and a structural model of full-length KcsA based on EPR spectroscopy[47] (PDB ID 1F6G) as input for homology modeling using MODELLER.[57] To conform to ssNMR data showing longer TM1 (TM = transmembrane) and C-terminal helices, the resultant model was subjected to a restrained simulated annealing protocol in CNS[58] in which all atoms were kept fixed except those in residues 20−24, 51−61, and 125−130, where helical structure in residues 22−24, 51−53, and 129 was enforced by applying α-helical dihedral angle restraints. Dihedral angles for residues 56−61 were kept close to their crystal structure values (see the Supporting Information for further details). For visualization, the PyMOL software was used (http://www.pymol.org).

Results and Discussion

2D and 3D ssNMR Correlation Experiments on KcsA-Kv1.3. In Figure 1, two-dimensional proton-driven $^{13}C-^{13}C$ spin diffusion (a) and NCACB (b) spectra of full-length [U]KcsA-Kv1.3 are shown. In addition, an NCOCA spectrum is given in the Supporting Information (Figure SI 1). In line with earlier studies,[24,48] spectral resolution is given by ^{13}C and ^{15}N line widths of 0.7 and 1.5 ppm, respectively, and compares favorably to ssNMR data obtained on protein microcrystals of globular proteins. While spectral resolution is high, resonance overlap due to the largely α-helical nature of the protein and high levels of occurrence of particular residue types (especially Ala, Arg, Leu, and Val) complicate the assignment process. For this reason, we complemented data from the fully isotope-labeled channel with data obtained on a sample ([R]KcsA-Kv1.3) reverse-labeled for some of the most abundant and spectrally overlapped amino acid types (Leu, Val) and for two of four aromatic residue types (Trp, Tyr), accounting for, in total, 29% of the entire amino acid sequence. This strategy facilitates assignment in the aromatic side chain regions[39,40] and significantly improves spectral resolution as shown in Figure 2, where a 2D PDSD experiment conducted on [R]KcsA-Kv1.3 under weak coupling conditions[52] reveals a variety of sequential $^{13}C-^{13}C$ connectivities (see also Figure SI 2, Supporting Information). Additionally, spectra from a C-terminally truncated sample were used to assist in identification of signals from residues 126−160 in spectra of full-length samples, and a 3D NCOCA spectrum was recorded to resolve sequential $^{15}N-^{13}C$ correlation information in an additional dimension. Data from $^{13}C-^{13}C$ correlation experiments were combined with $^{15}N-^{13}C$-type dipolar transfer experiments[51] to derive sequential resonance assignments classified into three levels of reliability (see the Supporting Information).

Figure 3 shows examples of the sequential assignment process. Combining $^{15}N-^{13}C\alpha$ correlation information obtained from 2D experiments (data not shown) with results of a 3D NCOCA experiment (Figure 3a) readily leads to assignments for residues Ala73 to Asp80 that contain the selectivity filter region of KcsA-Kv1.3. In addition, a large number of resonances could be identified by combining $^{15}N-^{13}C$ correlation experiments with sequential $^{13}C-^{13}C$ correlations from spectra obtained on [R]KcsA-Kv1.3. An example from the region around Gly99, which is assumed to contain the "gating hinge" for pH-dependent opening of the channel, is shown in Figure 3b and Figure SI 3 in the Supporting Information.

Overall, sequential assignments could be obtained for 94 (59%) of all 160 residues of KcsA-Kv1.3. A total of 73 of these fall within those parts of the protein seen in KcsA crystals[46] (PDB ID 1K4C, residues 22−124), while 21 additional residues from the intracellular N- and C-termini that were not resolved or not included in the crystal structure were identified. Assigned residues are indicated in Figure 1 and listed in Table SI 2 (Supporting Information).

Structural Analysis. Using the well-known correlation between secondary chemical shifts and secondary structure,[59–61] we can identify helical and nonhelical stretches of the protein in lipid bilayers and compare their distribution with those in crystalline and micelle preparations. Figure 4 shows residue-specific ssNMR secondary chemical shifts as bars, where positive values indicate helical secondary structure. Secondary structure elements of the crystal structure are provided

(51) Baldus, M. *Prog. Nucl. Magn. Reson. Spectrosc.* **2002**, *41*, 1–47.
(52) Seidel, K.; Lange, A.; Becker, S.; Hughes, C. E.; Heise, H.; Baldus, M. *Phys. Chem. Chem. Phys.* **2004**, *6*, 5090–5093.
(53) Baldus, M.; Petkova, A. T.; Herzfeld, J.; Griffin, R. G. *Mol. Phys.* **1998**, *95*, 1197–1207.
(54) Petkova, A. T.; Baldus, M.; Belenky, M.; Hong, M.; Griffin, R. G.; Herzfeld, J. *J. Magn. Reson.* **2003**, *160*, 1–12.
(55) Takegoshi, K.; Nakamura, S.; Terao, T. *Chem. Phys. Lett.* **2001**, *344*, 631–637.
(56) Lange, A.; Luca, S.; Baldus, M. *J. Am. Chem. Soc.* **2002**, *124*, 9704–9705.
(57) Sali, A.; Blundell, T. L. *J. Mol. Biol.* **1993**, *234*, 779–815.
(58) Brunger, A. T.; Adams, P. D.; Clore, G. M.; DeLano, W. L.; Gros, P.; Grosse-Kunstleve, R. W.; Jiang, J. S.; Kuszewski, J.; Nilges, M.; Pannu, N. S.; Read, R. J.; Rice, L. M.; Simonson, T.; Warren, G. L. *Acta Crystallogr., Sect. D: Biol. Crystallogr.* **1998**, *54*, 905–921.
(59) Saito, H. *Magn. Reson. Chem.* **1986**, *24*, 835–852.
(60) Wishart, D. S.; Sykes, B. D. *Nucl. Magn. Reson., C* **1994**, *239*, 363–392.
(61) Luca, S.; Filippov, D. V.; van Boom, J. H.; Oschkinat, H.; de Groot, H. J. M.; Baldus, M. *J. Biomol. NMR* **2001**, *20*, 325–331.

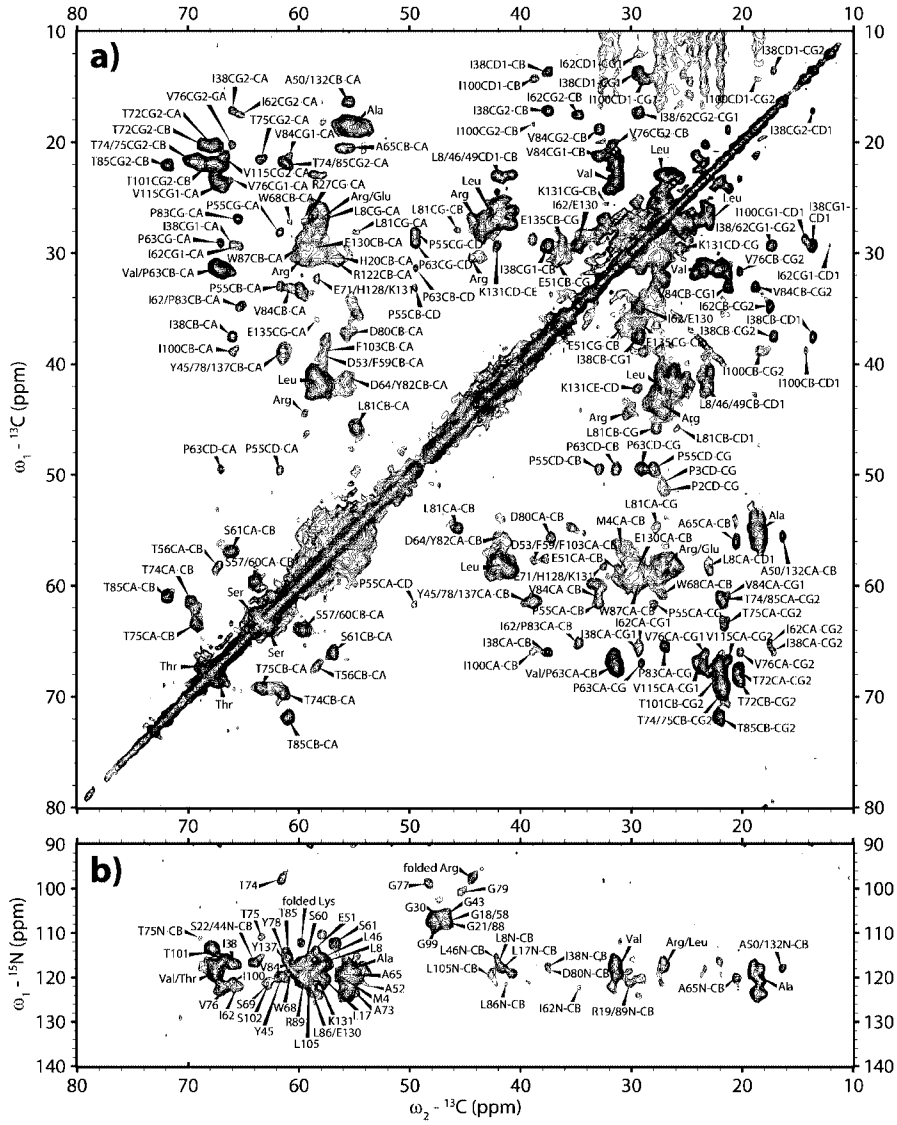

Figure 1. 2D ssNMR correlation spectra on [U]KcsA-Kv1.3 in liposomes recorded at 800 MHz ^{1}H Larmor frequency and 12.5 kHz MAS and with lipid bilayers in the liquid crystalline state. (a) Proton-driven ^{13}C−^{13}C spin diffusion spectrum. A spin diffusion mixing time of 20 ms was used. (b) NCACB correlation spectrum. SPECIFIC-CP (3 ms) was used for the ^{15}N−^{13}C transfer step; subsequently, DARR mixing (8 ms) was employed to obtain side chain ^{13}C resonances. Assigned residues as well as regions of significant overlap for certain residue types are indicated in both spectra. In the NCACB spectrum, peaks marked only with residue type and number represent ^{15}N−^{13}Cα correlations.

as reference at the top, while helical regions as apparent from our data are shown as horizontal bars at the bottom. In the transmembrane and extracellular parts of KcsA-Kv1.3, we find α-helical structure in the regions between residues 22 and 53, between residues 62 and 73, and from residue 86 to residue 116 or further, but not beyond residue 121. While we cannot infer the continuity of these helical segments in regions that could not be assigned, they correspond very closely to helical segments found in the crystal structure (transmembrane helices TM1 and TM2 and the pore helix). Some differences are apparent for TM1. Our data show strong indications for helical structure already at residue 22, while in the crystal structure, the TM1 helix begins only at residue 24, indicating a TM1 helix extending slightly longer at its N-terminus in lipid bilayers if continuity is assumed. The last residue exhibiting a strong α-helical secondary chemical shift is Asp53, pointing toward an extension of the TM1 helix by two residues (compared to the crystal structure) also at its C-terminus. The extracellular end of the TM1 helix and the turret loop connecting TM1 and the pore helix contain the Kv1.3 mutations in our sample and constitute the binding interface of the antibody used for crystal preparation,[46] such that structural differences in this region with respect to the crystal structure can be expected (see below and Figure SI 4, Supporting Information).

Further support for a slightly extended TM1 helix in liposomes comes from CHHC experiments[56] that probe through-space proton−proton contacts in an indirect manner. Three well-resolved cross-peaks from CHHC spectra recorded with ^{1}H−^{1}H mixing times of 250 and 500 μs and the CHHC spectrum with 500 μs proton mixing are shown in Figure 5. Correlations shown in (b) and (c) are consistent with contacts between residues in the turret loop of KcsA-Kv1.3. Corresponding proton−proton contacts in the crystal structure of KcsA (1K4C, with L59 instead of F59) are shorter than 3.5 Å and, in the absence of significant molecular motion (see below), would be expected to appear for significantly shorter ^{1}H−^{1}H mixing times (around

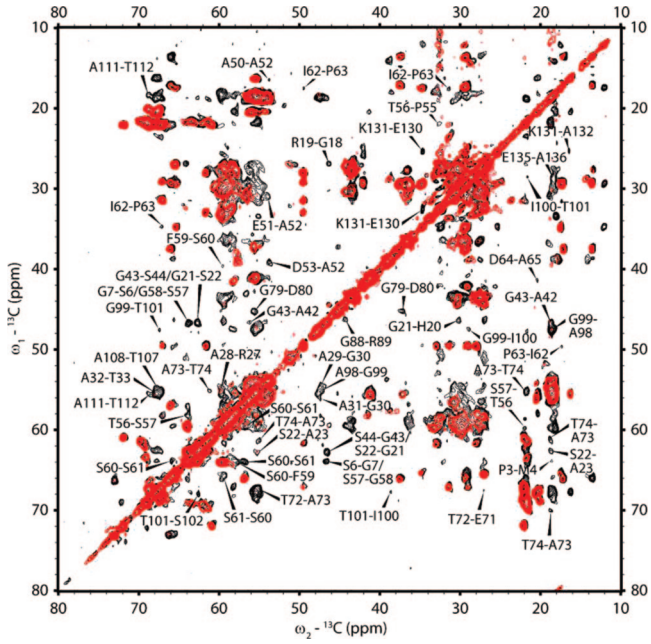

Figure 2. Overlay of proton-driven $^{13}C-^{13}C$ spin diffusion spectra of [R]KcsA-Kv1.3 recorded with 20 ms (red) and 150 ms (black) spin diffusion mixing times under weak coupling conditions[52] (800 MHz, 12.5 kHz MAS, lipid bilayer in the liquid crystalline phase). Assigned sequential correlations are indicated.

200−250 μs[32,62]). However, these cross-peaks are only seen for the longer $^{1}H-^{1}H$ mixing time of 500 μs. This result is in line with the assumption of a structural change in the turret region due to the presence of a longer TM1 helix. Furthermore, in the CHHC spectrum for 250 μs proton mixing, a cross-peak is found that is consistent with an (i, i + 3) contact typical for α-helical structure between residues Ala50 and Asp53 (Figure 5d). Taken together, chemical shift and proton−proton distance data give strong indications for a TM1 helix slightly longer than in the KcsA crystal structure.

In addition to structural alterations in the turret region, our data also clearly point to the presence of helical structure in the N-terminus, as seen from helical secondary chemical shifts observed for residues 4, 6−8, and 17−19, as well as in the C-terminus, beginning with residue 129. In line with EPR and solution-state NMR data, these results suggest that the N-terminus of KcsA-Kv1.3 contains an amphipathic α-helix that might serve as a membrane anchor. Similarly, the KcsA-Kv1.3 C-terminus appears to exhibit helical structure, possibly in the form of a helix bundle.[47,49,50]

To delineate the differences between previous solution-state NMR data on KcsA constructs and our ssNMR analysis in further detail, we conducted a comparative analysis in reference to solution-state NMR chemical shifts measured for KcsA constructs in foscholine[50] and SDS[49] micelles. In addition, we created a structural model of full-length KcsA-Kv1.3 based on the crystal structure of KcsA[46] (PDB ID 1K4C), an EPR model[47] of the intracellular N- and C-termini (PDB ID 1F6G), and our ssNMR data (see also Figure SI 5). The results are shown in Figure 6 as bar plots of Cα secondary chemical shifts for the different data sets and in Figure 7b,c as a color code of shift differences mapped onto the structural model of KcsA-Kv1.3.

(62) Lange, A.; Seidel, K.; Verdier, L.; Luca, S.; Baldus, M. *J. Am. Chem. Soc.* **2003**, *125*, 12640–12648.

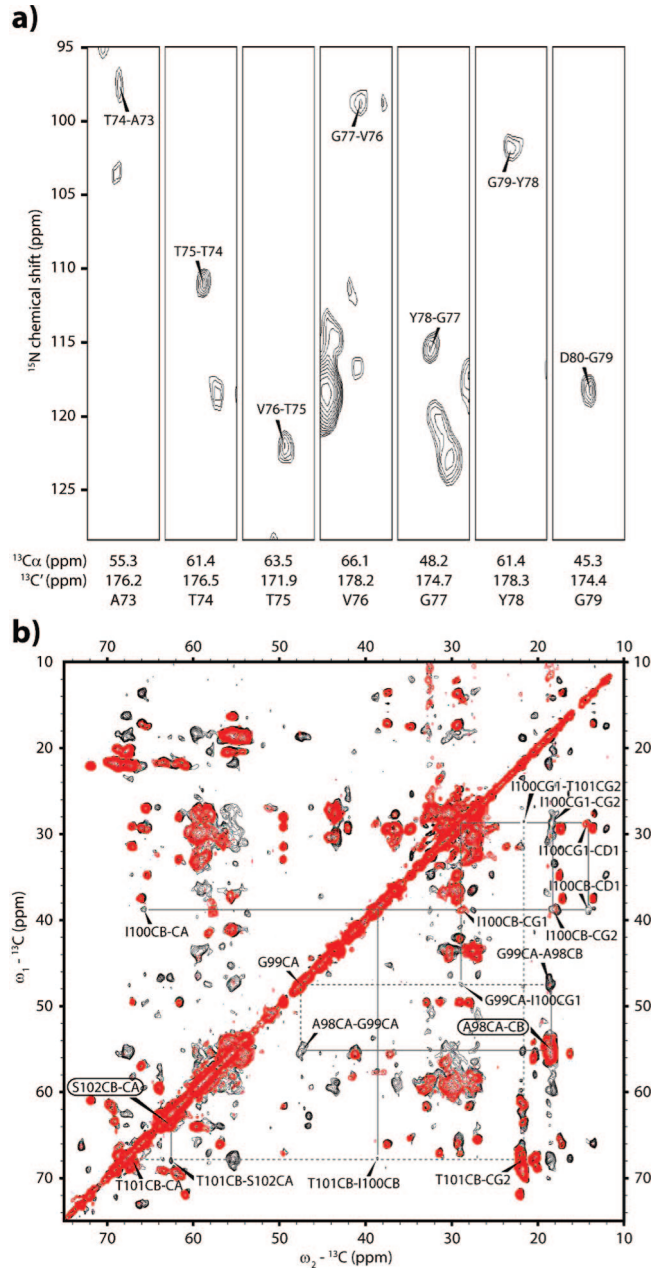

Figure 3. (a) Strip plot from a 3D NCOCA experiment recorded on [T]KcsA-Kv1.3 (800 MHz, 12.5 kHz MAS, lipid bilayer in the gel phase) showing $^{15}N_i-^{13}C_{i-1}$ correlations for residues in the selectivity filter region of KcsA-Kv1.3. Corresponding intraresidue $^{15}N_i-^{13}C_i$ correlations were obtained using 2D NCACB experiments. (b) Sample sequential walk using only intraresidue and sequential $^{13}C-^{13}C$ correlations. Spectra of [R]KcsA-Kv1.3 are shown under experimental conditions as in Figure 2, i.e., recorded with 20 ms (red) and 150 ms (black) mixing times. Resonances of individual residues along the sequential stretch are connected by solid or dotted lines. A sequential walk along the same residues including $^{15}N-^{13}C$ intraresidue and sequential information is shown in Figure SI 3 (Supporting Information).

Residues colored in red exhibit Cα chemical shift changes between solution- and solid-state NMR data larger than 2 ppm.

Figure 7a additionally shows which residues have been assigned and where the Kv1.3 mutations are located in KcsA-Kv1.3. Mutations are confined to the turret region where structural changes observed in reference to the crystal structure may, at least in part, be related to changes in protein sequence. On the other hand, the protein sequence and functional data for KcsA-Kv1.3 strongly suggest that the channel structure is

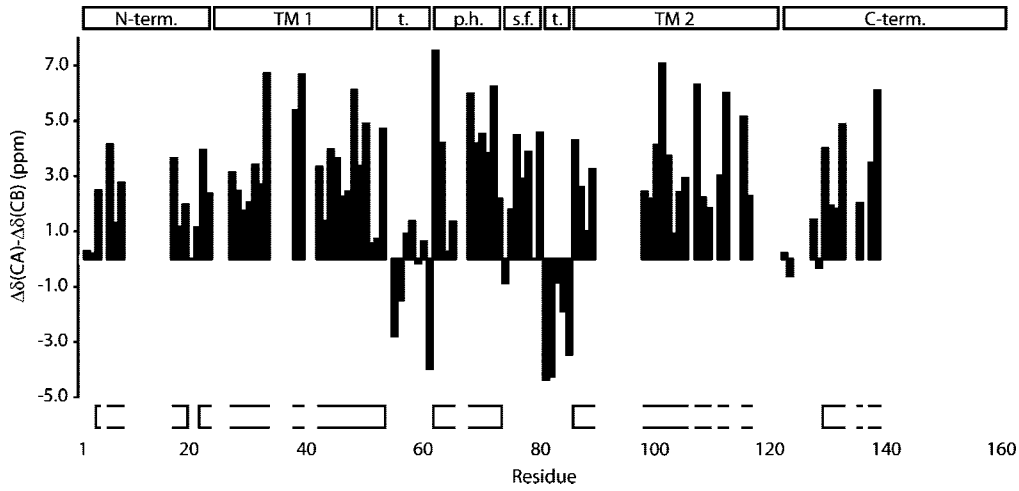

Figure 4. Secondary chemical shifts ($\Delta\delta(C\alpha)-\Delta\delta(C\beta)$) of KcsA-Kv1.3 with reference to average values taken from the Biological Magnetic Resonance Data Bank (BMRB; http://www.bmrb.wisc.edu). Positive values indicate helical structure. Secondary structure elements of the crystal structure are given as horizontal bars at the top (TM = transmembrane helix; t. = turret loop; p.h. = pore helix; s.f. = selectivity filter), as well as N- and C-terminal regions not covered by the crystal structure. Horizontal bars at the bottom show helical segments as seen by ssNMR.

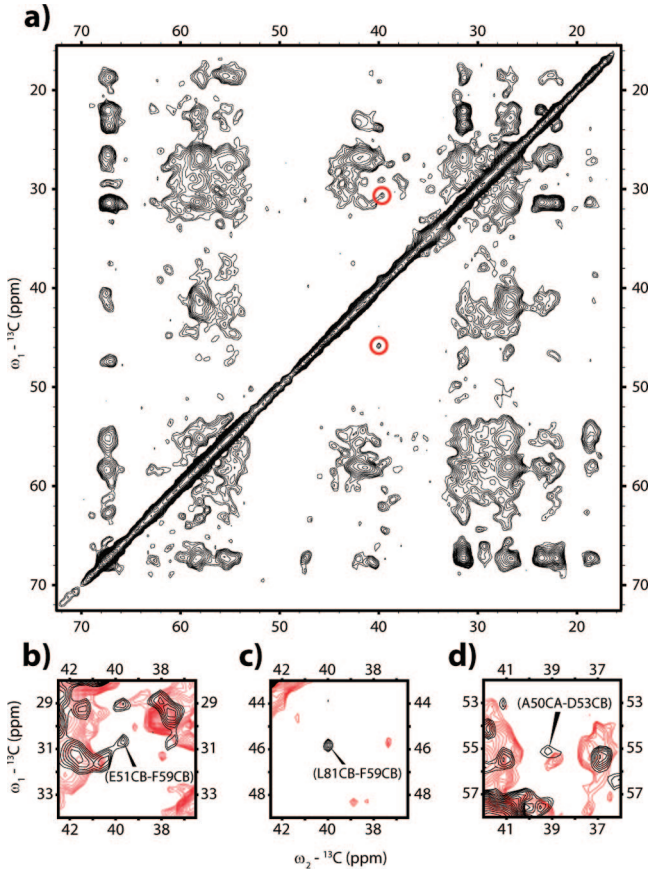

Figure 5. (a) CHHC spectrum of [U]KcsA-Kv1.3, recorded with a $^{1}H-^{1}H$ mixing time of 500 μs (600 MHz, 9.375 kHz MAS, lipid bilayer in the gel phase). Peaks enlarged in (b) and (c) are circled. (b–d) Spectral regions of the [U]KcsA-Kv1.3 CHHC spectrum shown in (a) (black, b, c) and of a CHHC spectrum with a $^{1}H-^{1}H$ mixing time of 250 μs (black, d), superimposed onto a $^{13}C-^{13}C$ spin diffusion spectrum (red) with a mixing time of 150 ms (800 MHz, 12.5 kHz MAS, lipid bilayer in the gel phase). Cross-peaks consistent with contacts within and between turret loops and with an (i, $i+3$) α-helical contact are shown in (b), (c) and (d), respectively. Labels in parentheses indicate that these peaks are not unambiguously assigned.

otherwise closely related to KcsA. A test of self-consistency in which we compared ssNMR secondary chemical shifts ($\Delta\delta(C\alpha)$) to values predicted for the structural model depicted in Figure 7 using SHIFTX[63] showed very good agreement between our assignments and the predictions within the accuracy limits of the program (Figure SI 5). Larger deviations are mostly confined to loop regions, suggesting that the structural model indeed captures the central structural features of KcsA-Kv1.3 in lipid bilayers.

Compared to solution-state NMR shifts, differences are seen for the N-terminus of TM1 and the intracellular C-terminal helix. In lipid bilayers, considering those residues for which we have assignments, helical structure in the C-terminus appears to be more pronounced and begins earlier in the sequence (residue 129), especially when compared to data measured in SDS micelles, where helical character becomes apparent at residue 142. This observation might be relevant for the tetrameric assembly of the channel, since the C-terminus has been shown to enhance thermal stability of the KcsA tetramer at neutral pH values.[64] On the other hand, our data indicate structural differences in the TM1 helix, where clear helical secondary chemical shifts are observed for all assigned residues between Ser22 and Gly30, while the TM1 helix begins only at residue 30 in micelles. This difference is likely of functional relevance, since residue His25 in this amino acid stretch has been shown to be crucial for the opening of the intracellular activation gate of KcsA occurring at low pH values.[65] While His25 could not be assigned from our data, it is surrounded by helical residues, unlike in micellar preparations, indicating a different, possibly helical, arrangement compared with that indicated by solution-state NMR data. Interestingly, our Cα secondary chemical shifts measured for two regions controlling ion conduction, i.e., the selectivity filter and the TM2 gating region, fit better to predictions using the KcsA crystal structure than to NMR values found for KcsA in SDS and foscholine micelles (Figure 7 and Figure SI 6 in the Supporting Information). In the selectivity filter, this difference may be related to different levels of potassium occupancy (R. Riek, personal communication). When

(63) Neal, S.; Nip, A. M.; Zhang, H. Y.; Wishart, D. S. *J. Biomol. NMR* **2003**, *26*, 215–240.
(64) Pau, V. P. T.; Zhu, Y.; Yuchi, Z.; Hoang, Q. Q.; Yang, D. S. C. *J. Biol. Chem.* **2007**, *282*, 29163–29169.
(65) Takeuchi, K.; Takahashi, H.; Kawano, S.; Shimada, I. *J. Biol. Chem.* **2007**, *282*, 15179–15186.

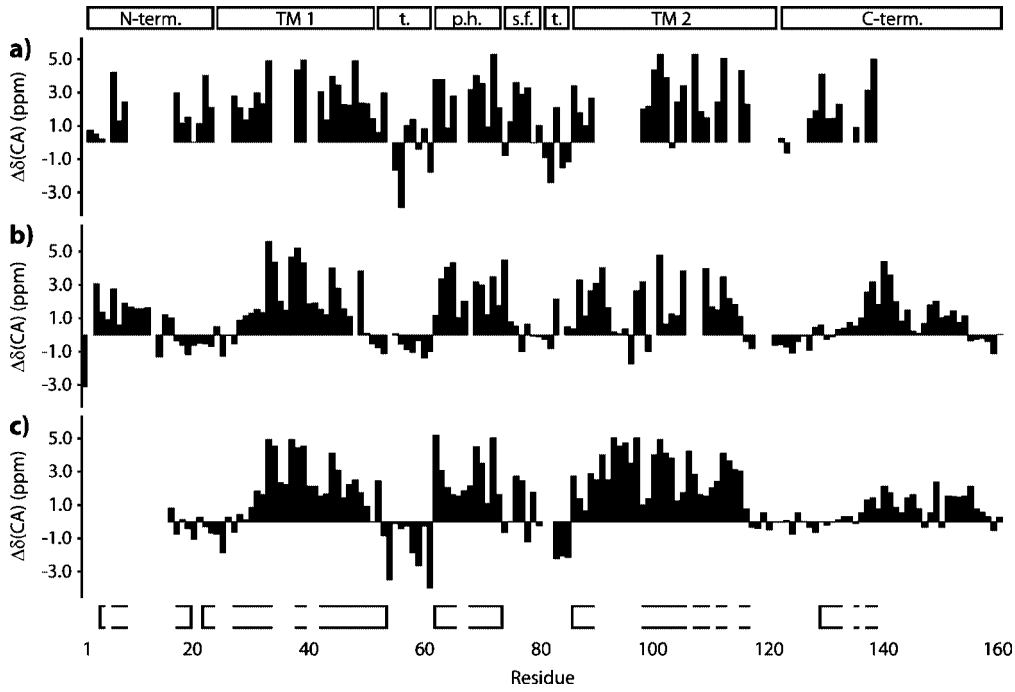

Figure 6. Comparison of Cα secondary chemical shifts. (a) KcsA-Kv1.3 in liposomes as seen by solid-state NMR. (b) Full-length KcsA studied by solution-state NMR in foscholine micelles.[50] (c) KcsA(16−160) measured by solution-state NMR in SDS micelles.[49] Positive values indicate helical structure. Secondary structure elements are given as in Figure 4.

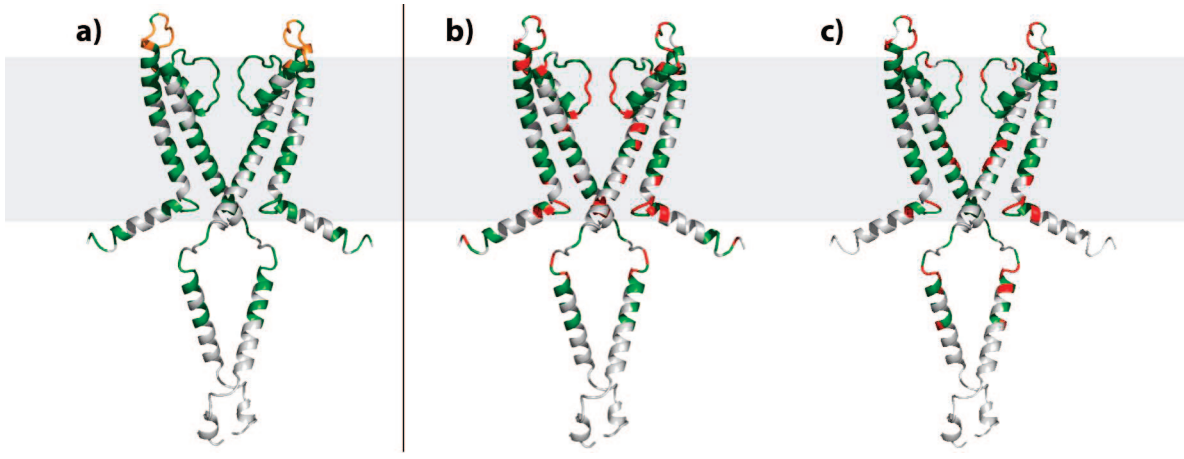

Figure 7. (a) Structural model of KcsA-Kv1.3 in lipid bilayers. Two of the four subunits have been removed for visual clarity. The gray rectangle reflects the approximate membrane environment. The color code indicates residues assigned by ssNMR. Among native KcsA residues, assigned ones are indicated in green, unassigned residues in gray. Residues mutated to Kv1.3 are colored orange, all of which except for Asp54 were assigned in lipid bilayers. (b, c) Differences in the Cα secondary chemical shift between ssNMR assignments on KcsA-Kv1.3 and solution-state NMR values for KcsA in foscholine micelles[50] (b) and SDS micelles[49] (c), color coded on the structural model of KcsA-Kv1.3. The color code shows residues with an agreement of $\Delta\delta$(Ca) within ±2 ppm in green, deviations greater than 2 ppm in red, and unassigned residues in gray.

comparing the total number of large chemical shift deviations (>2 ppm) between the solid- and solution-state NMR data sets in transmembrane regions and the selectivity filter, SDS micelle data seem to fit somewhat better to our solid-state NMR assignments (see Figure SI 6, Supporting Information). This might be surprising since SDS has been shown to destabilize the tetramer at low pH[66] and was used in conjunction with an elevated temperature of 50 °C. However, it is known that, for proper function, KcsA requires negatively charged lipids, as they are present in our asolectin liposome preparation.[67] Negatively charged detergents such as SDS might hence offer advantages compared to zwitterionic lipids such as foscholine to study functional aspects of the KcsA channel.

Finally, we also note a recent report describing ssNMR experiments and assignments for residues Val76−Asp80 and Pro83−Leu90 of the full-length KcsA channel precipitated from detergent micelles.[68] Compared to our results, aliphatic carbon shifts in the selectivity filter are similar. Significant differences

(66) Chill, J. H.; Louis, J. M.; Delaglio, F.; Bax, A. *Biochim. Biophys. Acta (BBA)—Biomembranes* **2007**, *1768*, 3260–3270.

(67) Valiyaveetil, F. I.; Zhou, Y.; MacKinnon, R. *Biochemistry* **2002**, *41*, 10771–10777.

(68) Varga, K.; Tian, L.; McDermott, A. E. *Biochim. Biophys. Acta (BBA)—Proteins Proteomics* **2007**, *1774*, 1604–1613.

between the two data sets exist for backbone nitrogen and carbonyl shifts in the selectivity filter, as well as for most residues in the second turret loop and at the beginning of the TM2 helix (residues 83−89; see Table SI 3, Supporting Information). Especially the latter differences may be attributable to the details of sample preparation and to differences in the amino acid sequence (our construct carries the mutation L90C in this region). On the other hand, the similarity of aliphatic carbon shifts in the selectivity filter between the two data sets suggests a similar conformation in liposomal and precipitated preparations. As can also be seen from the good agreement of our assignments with the KcsA crystal structure (see Figures SI 5b and SI 6 and ref 24), this conformation most likely corresponds to the conductive state of the selectivity filter as seen in high concentrations of potassium.

Molecular Mobility in KcsA-Kv1.3. All spectra of KcsA-Kv1.3 discussed so far were based on dipolar magnetization transfer, which is attenuated or even averaged out in the presence of significant molecular motion. SsNMR experiments on other membrane proteins have shown that loop regions can exhibit fast dynamics. Such protein segments are absent from dipolar transfer-based spectra but can be detected using scalar (through-bond) transfer sequences.[41,42] The presence or absence of significant levels of molecular mobility is of particular interest in the selectivity filter region. It has been a matter of debate whether ion selectivity in KcsA is a result of a relatively rigid selectivity filter that selects for potassium ions on the basis of their size using a well-defined protein structure[69] or whether the selectivity filter is actually a highly mobile region exhibiting "liquidlike" dynamics and selecting for potassium ions on the basis of electric field strength rather than their size.[70]

In KcsA-Kv1.3, experiments based on scalar transfer lead to signal sets that are dominated by lipid resonances (data not shown), arguing against the presence of protein segments that exhibit fast dynamics as seen, e.g., in sensory rhodopsin II.[42] On the contrary, signals from all residues comprising the selectivity filter (residues 75−79) and adjacent residues could clearly be identified in dipolar spectra, as well as almost all resonances in the turret loops (residues 54−61 and 80−85, Figure 8). For turret loop residues, this indicates that these residues can only exhibit limited molecular motion, even when not locked by antibody binding as in the crystal structure (see Figure SI 4, Supporting Information). This observation is consistent with solution-state NMR relaxation studies on KcsA in SDS micelles[71] where it was hypothesized that intersubunit contacts between turret regions could rigidify the structure of the turret loops. In the case of the selectivity filter, although further ssNMR experiments are required to exclude small amplitude molecular motions in our channel, our data strongly argue against a liquidlike structure that selects ions on the basis of electric field strength and support views in which ion selectivity is a result of ion size and protein structure.

Conclusions

We have shown that solid-state NMR experiments can be used to study the structure and dynamics of a 4 × 160 residue chimeric potassium channel in lipid bilayers. Compared to previous structural work on the closely related KcsA channel,

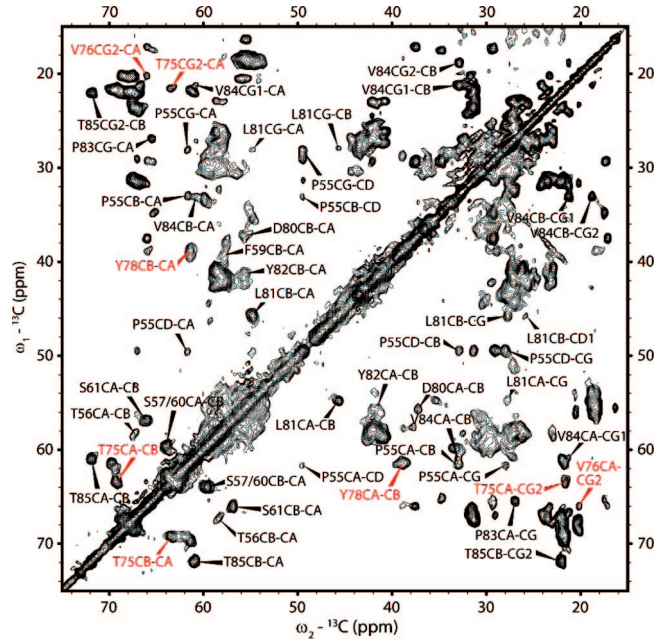

Figure 8. Proton-driven $^{13}C-^{13}C$ spin diffusion spectrum of [U]KcsA-Kv1.3 (800 MHz, 20 ms spin diffusion mixing time, 12.5 kHz MAS, lipid bilayer in the liquid crystalline phase). Assignments indicate correlations arising from residues in the selectivity filter (red) and turret loops (black). Correlations for Gly77 and Gly79 in the selectivity filter are seen in the carbonyl region and in $^{15}N-^{13}C$ correlation spectra (not shown).

our data indicate that transmembrane helix 1 is slightly longer at both ends, especially at its N-terminus, when compared to the length apparent from NMR data in micelles. Consistent with results from an EPR study, we find clear evidence for the formation of an N-terminal α-helix. Although ssNMR resonance assignment in the C-terminus is still incomplete, our data strongly suggest helical structure in the C-terminus as well (starting from residue 129), consistent with an EPR structural model proposing a four-helix bundle in this region. The clear presence of resonances from the turret loops and selectivity filter in dipolar spectra suggests reduced mobility in these regions, speaking in favor of a mechanism for ion selectivity based on protein structure and ion size.

Although 11 mutations are present in our construct, structural and functional evidence suggests that KcsA-Kv1.3 and the KcsA channel are structurally closely related.[72] The observed differences are hence in line with increasing evidence that protein structure and function can be influenced by the surrounding membrane environment. Structural differences between bilayer preparations and micellar systems may, in part, reflect the fact that micelles have stronger curvature and lack the asymmetry and the closely packed headgroups of a bilayer.[6] In line with previous evidence,[67] our work also points to the potential influence of lipid charges on the structure and function of membrane proteins.

In this study, we have reported assignments for 59% of the residues of the entire protein and 71% of its putative transmembrane and extracellular regions. Advanced labeling schemes, possibly involving cell-free-based expression systems,[73] are

(69) Noskov, S. Y.; Berneche, S.; Roux, B. *Nature* **2004**, *431*, 830–834.
(70) Lockless, S. W.; Zhou, M.; MacKinnon, R. *PLoS Biol.* **2007**, *5*, 1079–1088.
(71) Chill, J. H.; Louis, J. M.; Baber, J. L.; Bax, A. *J. Biomol. NMR* **2006**, *36*, 123–136.
(72) Ader, C.; Schneider, R.; Hornig, S.; Velisetty, P.; Wilson, E. M.; Lange, A.; Giller, K.; Ohmert, I.; Martin-Eauclaire, M. F.; Trauner, D.; Becker, S.; Pongs, O.; Baldus, M. *Nat. Struct. Mol. Biol.* **2008**, in press.
(73) Trbovic, N.; Klammt, C.; Koglin, A.; Lohr, F.; Bernhard, F.; Dotsch, V. *J. Am. Chem. Soc.* **2005**, *127*, 13504–13505.

likely to improve the prospects of complete ssNMR assignments in larger membrane proteins in lipid bilayers. In the current context, an α-helical protein was investigated. Similar studies may be important for β-barrel proteins that are under investigation by solution-state (see, e.g., refs 16 and 74) and solid-state NMR.[38,75] Such studies not only provide the basis for ssNMR-based structural studies in membrane proteins of unknown structure but also underline the importance of ssNMR for understanding functional aspects of membrane-embedded proteins even if structural data from X-ray crystallography or solution-state NMR are available.

Acknowledgment. This work was funded in part by the DFG (Grants Ba 1700/8-1 and Po 137/38-1). R.S. thanks the DFG graduate school 782 "Spectroscopy and Dynamics of Molecular Coils and Aggregates" for a Ph.D. fellowship. C.A. gratefully acknowledges financial support by the Fonds der Chemischen Industrie (FCI). We are grateful to A. Bax and R. Riek for providing solution-state NMR resonance assignments of KcsA constructs in micelles.

Supporting Information Available: NCOCA $^{15}N-^{13}C$ correlation spectrum of KcsA-Kv1.3, comparison of proton-driven $^{13}C-^{13}C$ spin diffusion spectra of [U]- and [R]KcsA-Kv1.3, sequential walk through amino acid residues 98−102 of KcsA-Kv1.3 including $^{15}N-^{13}C$ correlation spectra, illustration of antibody binding to the turret region in the KcsA crystal structure, composition of the structural model of KcsA-Kv1.3 and consistency check of our assignments with the model, comparison of Cα secondary chemical shifts in the KcsA-(Kv1.3) selectivity filter and putative gating region between solid-state and solution-state NMR data and shift predictions from the crystal structure, list of KcsA-Kv1.3 spectra used for assignment, solid-state NMR resonance assignments for KcsA-Kv1.3 in liposomes, and comparison between solid-state NMR assignments on KcsA-Kv1.3 in liposomes and KcsA precipitated from detergent micelles. This material is available free of charge via the Internet at http://pubs.acs.org.

JA800190C

(74) Liang, B.; Tamm, L. K. *Proc. Natl. Acad. Sci. U.S.A.* **2007**, *104*, 16140–16145.
(75) Mahalakshmi, R.; Franzin, C. M.; Choi, J.; Marassi, F. M. *Biochim. Biophys. Acta (BBA)—Biomembranes* **2007**, *1768*, 3216–3224.